Spatiotemporal variability of land surface temperature in north-western Ethiopia

Getachew Bayable (bayable.geta@gmail.com)
Bahir Dar University
Getnet Alemu
Oda Bultum University

Research Article

Keywords: Elevation, LST, Mann-Kendall Trend Test, MODIS, Sen's slope

Posted Date: May 14th, 2021

DOI: https://doi.org/10.21203/rs.3.rs-432543/v1

Version of Record: A version of this preprint was published at Environmental Science and Pollution Research on August 10th, 2021. See the published version at https://doi.org/10.1007/s11356-021-15763-9.

Spatiotemporal variability of land surface temperature in north-western Ethiopia

Getachew Bayable Tiruneh[1*], Getnet Alemu[2]

[1]Department of Natural Resource Management, Bahir Dar University, Bahar Dar, Ethiopia
[2]Department of Environmental Science, Oda Bultum University, Chiro, Ethiopia

*Corresponding author: bayable.geta@gmail.com

Abstract

The aggravating deforestation, industrialization and urbanization are increasingly becoming the principal causes for environmental challenges worldwide. As a result, satellite-based remote sensing helps to explore the environmental challenges spatially and temporally. This investigation analyzed the spatiotemporal discrepancies in Land Surface Temperature (LST) and the link with elevation in Amhara region, Ethiopia. The Moderate Resolution Imaging Spectroradiometer (MODIS) LST data (2001-2020) was used. The pixel-based linear regression model was employed to explore the spatiotemporal discrepancies of LST changes pixel-wise. Furthermore, Sen's slope and Mann-Kendall were used for determining the extent of temporal shifts of the areal average LST and evaluating trends in areal average LST values, respectively. Coefficient of Variation (CV) was calculated to examine spatial and temporal discrepancies in seasonal and annual LST for each pixel. The distribution of average seasonal LST spatially ranged from 43.45-16.62℃, 39.89-14.59℃, 50.39-21.102℃ and 43.164-20.39℃ for autumn (September-November), summer (June-August), spring (March-May) and winter (December-February) seasons, respectively. The seasonal LST CV varied from1.096-10.72%, 0.7–11.06%, 1.29–14.76% and 2.19–10.35% for average autumn, summer, spring and winter seasons, respectively. The seasonal spatial LST trend varied from -0.7-0.16, -0.4-0.224, 0.6-0.19 and -0.6-0.32 for average autumn, summer, spring and winter seasons, respectively. Besides, the annual spatial LST slope varied from -0.58-0.17. An insignificantly declining trend in LST shown at 0.036℃ yr^{-1}, 0.041℃ yr^{-1}, 0.074℃ yr^{-1} , 0.005℃ yr^{-1} in autumn, summer, spring and winter seasons ($P<0.05$), respectively. Moreover, the annual variations of mean LST decreased insignificantly at 0.046℃ yr^{-1}. Generally, the LST is tremendously variable in space and time and negatively correlated with an elevation.

Keywords: Elevation; LST; Mann-Kendall Trend Test; MODIS; Sen's slope

1. Introduction

Anthropogenic activities are becoming the principal cause for increasing greenhouse gases which results in a devastating environmental problems. The growing increment in population leads to increasing deforestation, forest degradation, agriculture, urbanization and industrialization. This event has extensive effect on ozone depletion which in turn boosts land surface temperature (LST). Besides, the disruption of global climatic condition, biological diversity and energy consumption are becoming common (Güneralp et al., 2017; Yang et al., 2020). Because, a significant amount of natural and plantation forests, shrub lands and croplands are destroyed and

replaced by artificial impervious surfaces which could be the source of an enormous environmental influences on this planet (Miles & Esau, 2020; Zhou et al., 2016; Fabeku & Balogun, 2018; Jiang et al., 2015). Specifically, this situation causes a fall in evapotranspiration through photosynthesis, increase in run-off and LSTs which in turn increases the occurrence of Urban Heat Island (UHIs) (Farina, 2012; Ibitoye et al., 2017; Singh et al., 2014; Ye et al., 2017). UHI refers to an intensification in LST and has a substantial effect on urban climate, human wellbeing, biodiversity, and sustainable development (Chen et al., 2017; Qiao et al., 2020; Yang et al., 2020). In short, UHI can be expressed as the situation where an urban environment has higher temperature than rural environment (Aina et al., 2017). Global warming is happened by absorption of incoming radiation from sunlight in a huge amount and re-radiating less while its cooling occurs when the outgoing solar radiation be significant. No country can be immune from the adverse global warming impacts since it has no geographical boundary so that it requires the collective efforts of every nation.

LST is the crucial element in the investigation of climate in urban area. Because, it is very pertinent for the assessment of climate change and UHIs (Amiri et al., 2009; Khorchani et al., 2018; Mirzaei et al., 2020). It helps to evaluate temperature dynamics of the earth's surface which is intensively correlated with climate change based on long-term data (Jiang et al., 2015; Peng et al., 2018; Zhu et al., 2018). The previous studies stated that LST change is highly linked with land-use/land cover change. When a significant amount of GHGs are released, naturally available GHGs would be denser so that abundant amount of outgoing solar radiation would be blocked and will cause LST increment. Though benefits like getting warmness and obtaining longer time growing season for crops are obtained from increasing temperature, it causes a substantial socioeconomic and environmental challenges. Consistent assessments of LST discrepancies are vital for recognizing land surface energy budget and its interactions with the atmosphere properly (Maffei et al., 2018; Mildrexler et al., 2018; Thorne et al., 2016). LST can be expressed as an indicator of interactions among the components of climate system. It further shows the thermal reaction to the urban coverage, height of construction, land surface coverage and energy consumption (Yang et al., 2020; Li et al., 2013; Khandelwal et al., 2017; Miles & Esau, 2020).

Temperature can be measured by means of traditional observation and remote-sensing techniques. Remote sensing is among the indirect approaches which is helpful to evaluate the LST (Shwetha & Kumar, 2016). In recent times, it has become effective method to obtain data at a large-scale spatial and temporal coverage for investigating the spatiotemporal changes in vegetation, land-use/land cover and LST (Berger et al., 2017; Li et al., 2013; Tomlinson et al., 2011). Moreover, it is increasingly helps to assess biological, physical and other features in this planet (Li et al., 2020; Qureshi et al., 2020). LST is an essential constituent of climate system which is influenced prominently by interactions of the atmosphere and earth's surface. The spatiotemporal discrepancies in LST and its consequences are wide-ranging across urban and rural environments. In equatorial and temperate regions, urban areas usually experienced higher surface temperatures than rural areas, unlike arid areas. This is mainly because of the intervention by humans and relatively low natural vegetation (Parvez et al., 2019). A number of studies showed that remote sensing has the benefit of delivering uninterrupted, greatest quality

and real data of large areas as compared to meteorological stations data (Khanal et al., 2020; Li et al., 2013; Ngie et al., 2014). Ground-based meteorological stations LST data are limited at worldwide scale. Due to this, it is generally considered as inadequate to examine its discrepancies at a higher spatial scale (Noureldeen et al., 2017).

Numerous investigations have been done regarding to the LST spatiotemporal discrepancies by means of MODIS data in Asian and West African countries. However, limitations of such studies are witnessed in Ethiopia, particularly over Amhara region. Deforestation is aggregated time to time because of the growing population in this region. This circumstance influences global warming. This investigation, therefore, would offer vital information regarding to the LST dynamics and its link with elevation. It further helps for drought assessment. Therefore, this investigation analyzed the spatiotemporal discrepancies of LST and its link with elevation.

2. Materials and methods

2.1 The study area

Amhara region is situated between 8°45′N to 13º45′N latitude and 35°46′ to 40°25′E longitudes (Fig. 1). The area coverage was expected to be 156, 960 km^2, and its altitudes found between 513 m a.s.l to 4462 m a.s.l. Most districts are found above 1,500 m a.s.l. According to Ayalew et al. (2012), the yearly mean temperature ranges from 15-21°C. Rain-fed farming is the predominant livelihood source of the communities. About 89% of the people are involved principally in mixed agriculture (Ayalew et al., 2012).

Fig. 1: Study Area Map

2.2 Methods

2.2.1 Data and preprocessing

The MODIS (Moderate Resolution Imaging Spectroradiometer) data was used. According to Justice et al. (1998), MODIS refers to multispectral device on the Aqua and Terra satellites that quantity high-spatial-resolution constituents of climate system at 36 visible and ultraviolet frequencies with 0.4–14.4mm spectral range. Now a days, MODIS images are increasingly employed to develop numerous data for environmental investigations and monitoring, including LST products. A Terra product was used. Because, it contains longer time series data.

The monthly products on a 0.05° topographical grid (MOD11C3) were used although a one km daily spatial resolution data was available. This was done because the accessibility and trustworthiness of LST data increase with spatial and temporal aggregation (Bosilovich, 2006; X. Li et al., 2018). Version 6 MOD11C3 LST data (2001-2020) were downloaded from USGS LPDAAC ftp server (https://lpdaac.usgs.gov/data_access/data_pool). Moreover, the quality flag in MOD11C3 was employed to screen the observations with reduced quality. Preprocessing comprised subsetting, reprojecting, and eliminating false data-points. These false data-points incorporate pixels influenced by atmospheric disturbances including clouds. Several researchers pointed out the significance of screening cloud-contaminated data-points in time series environmental and climatic data investigation (Julien et al., 2006; Julien & Sobrino, 2009).

Besides, Shuttle Radar Topographic Mission (SRTM) Digital Elevation Model (DEM) was used and acquired from the United States Geological Survey (USGS) (https:/earthexplorer.usgs.gov/).

2.2.2 Trend analysis

The pixel-based linear regression model was employed to evaluate the trends of LST changes pixel-wise in space and time using the seasonal and annual observations (2001-2020) (Eq.1). The seasons are classified as: Autumn from September to November (SON), summer from June to August (JJA), spring from March to May (MAM) and winter from December to February (DJF) (Alemu & Bawoke, 2019). The negative and positive LST slope values indicate decreasing and increasing trend, respectively (Qian et al., 2016;.NourEldeen et al., 2020). In this investigation, the dependent and explanatory variables were LST and year, respectively. The pixel-wise analysis in LST trend was calculated using Eq.1 (Nusseiba et al., 2020, Zhang et al., 2011).

$$\text{Slope} = \frac{n\times\sum_{i=1}^{n} LSTi\times ti-(\sum_{i=1}^{n} LSTi)(\sum_{i=1}^{n} ti)}{n\times\sum_{i=1}^{n} ti^{2}-(\sum_{i=1}^{n} ti)^{2}} \qquad \text{(Eq.1)}$$

where LSTi refers to land surface temperature in year i, n refers to length of time (n=20) and ti refers to an index number for 2001 to 2020 (1-20).

In addition, Sen's slope was computed to determine magnitude of temporal shifts of the areal average LST. Several studies indicated that this approach is influenced in less extent by missing data and outliers unlike linear regression (Fernandes & Leblanc, 2005; Porter et al., 2002). When linear trend is available, degree of the monotonous trend could be calculated and determined using Sen's slope estimator shown by Eq.2 (Sen, 1968):

$$\beta = \text{median}(\frac{yj-yi}{j-i}) \qquad \text{(Eq.2)}$$

where β is the median of slope values between the yi and yj data measurements in phases i and j (i < j), respectively. The negative and positive value of β show downward an upward trend, respectively. Besides, the sign and value of β indicate the course and steepness of the trend, respectively.

Furthermore, Non-Parametric Mann-Kendall trend test method was executed to evaluate the trends in areal average LST values over Amhara region. It is usually employed to assess monotonic trends of large time series climatic, environmental and hydrological data. It is commonly affected in some extent when data is missing and distributed unevenly. Moreover, it is less vulnerable to outliers. This is for the reason that ranks of observations are considered unlike their actual values (Libiseller & Grimvall, 2002). The null hypothesis (H0) was there is no trend. Meaning, the Yi data are randomly ordered and tested against the alternative hypothesis (H1). The Mann-Kendall statistics (S) was calculated using the formulae developed by Mann (1945) and shown below by Eq.3:

$$S = \sum_{i=1}^{n-1}\sum_{j=i+1}^{n} \text{Sign}(yj - yi) \qquad \text{(Eq.3)}$$

where Yi and Yj are consecutive data values for n-length data and

$$\text{Sign}(yj - yi) = \begin{cases} 1 \text{ if } (yj - yi) > 0 \\ 0 \text{ if } (yj - yi) = 0 \\ -1 \text{ if } (yj - yi) < 0 \end{cases} \quad \text{(Eq.4)}$$

When the data are distributed identically and independently, Sen's slope estimator mean is zero, and Sen's slope estimator variance was computed using the formulae shown below by Eq.5:

$$\text{Var(S)} = \frac{1}{18}\left[n(n-1)(2n+5) - \sum_{i=0}^{m} \text{ti}(\text{ti}-1)(2\text{ti}+5)\right] \quad \text{(Eq.5)}$$

where n refers to the length of data, m refers to tied groups number in time series (a tied group refers a group of sample data with similar value), and ti refers to the number of data points in the i^{th} group

The Z statistics were computed using Eq.6:

$$Z = \begin{cases} \frac{S+1}{\sqrt{\text{Var (S)}}} & \text{for } S < 0 \\ 0 & \text{for } S = 0 \\ \frac{S-1}{\sqrt{\text{Var (S)}}} & \text{for } S > 0 \end{cases} \quad \text{(Eq.6)}$$

To test the monotone trends, a significance level (α=0.05) was used. The decision for the two-tail hypothesis test was made by comparing the calculated Z with critical values. The H0 is accepted if the critical value is greater than the absolute value of calculated Z or if the p-value is higher than the selected significance level. On the contrary, the H0 is rejected if and only if the absolute value of the calculated Z is greater than the critical value. Once the H0 is rejected, the value of Z is negative and positive for declining and increasing trends, respectively (Mesbah, 2013). Furthermore, it was considered as statistically significant if the H1 is accepted.

2.2.3 Analysis of Coefficient of Variation (CV)

The LST variability for each pixel was analyzed seasonally and annually in space and time by computing the CV (Gidey et al., 2018). The analysis of CV was undertaken to evaluate the annual and seasonal LST discrepancies relative to mean percentage (2001-2020). The CV was calculated using the formulae shown below:

$$\text{CV}(\%) = 100\left(\frac{\sigma}{\overline{x}}\right) \quad \text{(Eq.7)}$$

where CV refers to the coefficient of variation value of LST, σ refers to the standard deviation of LST and $\overline{x}$ is the long-term mean of LST.

3. Results and discussion

3.1 Distribution of LST

The spatial distribution in average seasonal LST (2001-2020) spatially ranged from 43.45-16.62°C, 39.89-14.59°C, 50.39-21.102°C and 43.164-20.39°C for autumn, summer, spring and winter, respectively (**Fig. 3**). During spring and winter seasons, the highest LST experienced in western, north-western, and north-eastern districts. In opposition, the lowest LST values shown in southern and eastern districts. Moreover, the eastern, north-eastern, and north-western districts of the region showed the highest LST in autumn and summer seasons. In contrast, the central,

southern, and northern districts experienced the lowest LST (**Fig. 3**). The reason might be associated with most of eastern, north-eastern, and north-western districts had lower elevation **(Fig. 2).** In opposition, most of the central, southern, and northern districts had higher elevation. This result is in line with results of several studies (Z. Qiao et al., 2020; He et al., 2018; Phan et al., 2018; X. Peng et al., 2020) who revealed that areas with higher elevation are recognized by lower LST. LST for spring season was greater than other seasons. Besides, average annual LST spatial distribution ranged from 41.976℃-18.565℃ (**Fig. 3**).

Fig.2: Elevation across different zone **(a)** and elevation of the region **(b)**

Fig. 3: Spatial distribution of average winter (DJF) LST **(a)** mean spring (MAM) LST **(b)** mean summer (JJA) LST **(c)** mean autumn (SON) LST **(d)** and mean annual LST **(e)** (2001-2020)

3.2 Spatiotemporal Variability in LST

Fig. 4 shows the seasonal LST distribution CV (%) in space. The seasonal LST CV ranges from 1.096-10.72%, 2.19–10.35%, 1.29–14.76% and 0.7–11.06% for average autumn, summer, spring and winter seasons, respectively (2001–2020). For winter season, the maximum inter-annual discrepancies in LST shown in the eastern district. In opposition, the northern, central, and western parts showed less inter-annual variability. Moreover, the maximum inter-annual variability experienced in eastern, south-western, and northern districts in spring season. In opposite, less inter-annual discrepancies experienced in northern eastern, north-western, and western districts. Besides, the eastern, southern, and north-eastern districts showed the maximum inter-annual variability. Whereas, north-western and north-eastern districts showed the lowest inter-annual discrepancies in autumn season. In opposition, the maximum inter-annual variability experienced in southern, central, and western parts in summer season. However, less inter-annual discrepancies experienced in eastern, north-western, and south-western districts. The CV of LST for spring season (1.29 %< CV<14.76%) was greater than other seasons and also the maximum inter-annual discrepancies of LST recorded in spring season than other seasons.

Furthermore, the annual LST CV (%) distribution in space is presented in **Fig. 4 e**. The annual LST CV (2001-2020) ranged from 0.97-10.37%. The maximum inter-annual discrepancies experienced in eastern, northern and south-western districts. In opposite, less inter-annual variability was detected in western, north-western and north-eastern districts. Vegetation cover change of surfaces might be the reason for the maximum inter-annual discrepancies in eastern, northern, and south-western districts. Because, the earth surface's thermal properties with high vegetation are different from earth surfaces with low vegetation cover. The rise of vegetation cover is favorable to increasing soil moisture content, which can reduce soil erosion and desertification. In the equatorial and temperate regions, the areas with low vegetation cover are generally known by higher surface temperatures than the areas with high vegetation cover (Cai et al., 2016; Xiao et al., 2018; Ye et al., 2017).

Fig. 4: The spatial distribution of LST CV of the winter season **(a)** spring season **(b)** summer season **(c)** autumn season **(d)** and annual LST (e) (2001-2020)

3.3 Spatiotemporal Trend

Fig. 5 depicts the seasonal spatial LST trend of Amhara Region. The seasonal spatial LST trend varied from -0.6-0.19, -0.4-0.224, -0.7-0.16 and -0.6-0.32 for average autumn, summer, spring and winter seasons, respectively (2001–2020). During spring and winter seasons, negative LST slope values experienced in western, mid-northern, and central district. However, positive slope values experienced in eastern, southern, south-western, and north-western districts. Besides, the negative LST slope values also experienced in southern, eastern, central, and mid-northern districts while positive slope values were experienced in western, south-western, north-western, and north-eastern districts in autumn and summer seasons. The annual spatial LST slope varied from -0.58-0.17 **(Fig. 5).** Negative slope were found in central, mid-western, and mid-northern districts. However, positive slope were found in north-western, north-eastern, southern, eastern, and south-western districts in annual LST. Increasing trend of the annual LST in north-western, north-eastern, southern, eastern, and south-western districts could be associated with the influences of anthropogenic activities like agricultural expansion, deforestation, and variation of elevation. Several studies (Berger et al., 2017; Jiang et al., 2015; H. Yang et al., 2020; Fabeku et al., 2018; Qiao et al., 2020; Phan et al., 2018) stated a strong negative association is available elevation and vegetation with LST.

Fig. 5: The spatial LST trend of winter season (a) spring season (b) summer season (c) autumn season (d) and annual LST (e) (2001-2020)

On the monthly basis, the trends of spatial average LST decreased insignificantly (2001-2020) in all months except in January, March, August, and September ($P<0.05$) (**Table 1**). Similarly, the seasonal discrepancies of areal average LST are presented in **Fig. 6**. LST decreased insignificantly at 0.036℃ yr^{-1}, 0.041℃ yr^{-1}, 0.074℃ yr^{-1} and 0.005℃ yr^{-1} in autumn, summer, spring and winter seasons, respectively at 5% significance level during the analyzed periods (**Table 1 and Fig. 6**). Moreover, annual variations of spatial average LST decreased insignificantly at 0.046℃ yr^{-1}. On the contrary, inter-annual discrepancies of autumn, summer, spring and winter seasons LST increased insignificantly from 2001-2020. However, the inter-annual discrepancies of annual LST increased significantly (**Fig. 7 and Table 2**).

Table 1: The Non-Parametric Mann-Kendall trend of areal average LST (℃) (2001-2020)
Fig. 6: Yearly variation of average seasonal and annual LST (2001-2020)
Fig. 7: Inter-annual variability of seasonal and annual LST (2001-2020)
Table 2: The Non-Parametric Mann-Kendall trend of STD of LST (2001-2020)

4. Conclusions

This study evaluated the spatiotemporal discrepancies of LST and its link with elevation using a MODIS LST dataset (2001-2020) in Amhara region. The results pointed out that LST is enormously variable in space and time. Specifically, the results show the highest spatial average seasonal LST distribution in spring season (50.39-21.102℃). Similarly, the highest seasonal LST CV (1.29–14.76%) experienced in spring season. The seasonal spatial LST trend varies from -0.6-0.19, -0.4-0.224, -0.7-0.16 and -0.6-0.32 for mean autumn, summer, spring and winter seasons, respectively. Furthermore, the annual spatial LST slope varies from -0.58-0.17. The western, mid-northern, and central areas show a general warming trend in winter and spring

seasons. Besides, southern, eastern, central, and mid-northern parts show a warming trend during summer and autumn seasons. In contrast, a general decreasing trend were found in the eastern, southern, south-western, and north-western districts during winter and spring seasons. A decreasing trend also experienced in western, south-western, north-western, and north-eastern districts in summer and autumn seasons. Central, mid-western and mid-northern districts show a decreasing trend while the north-western, north-eastern, southern, eastern and south-western districts show increasing trend in LST annually. Rate of decrement trend in spatial mean LST lies between 0.005°C yr^{-1} and 0.074°C yr^{-1}. The spring season LST trend is insignificantly decreasing greater than other seasons at 0.074°C yr^{-1} ($P<0.05$). The annual variations of mean LST decreased insignificantly at the rate of 0.046°C yr^{-1}. Moreover, a negative correlation was observed between elevation and LST. In general, the present study presents the LST dynamics over Amhara region. The findings would provide invaluable information to plan and implement appropriate adaptation and mitigation strategies by the experts of forestry, environment, and climate change.

Declarations

Author contribution statement

Getachew Bayable Tiruneh: Participated in data analysis, interpretation and writing the paper.

Getnet Alemu Desta: Participated in data analysis, interpretation and writing the paper.

Funding statement

The researchers don't obtain any financial support.

Competing interest statement

The researchers confirm no conflict of interest.

Additional information

No extra information is available.

Acknowledgments

We acknowledged our colleagues for encouraging us.

Consent to Publish

Not applicable

Consent to Participate

Not applicable

Ethical Approval

Not applicable

Availability of Data and Materials

The data for this research can be accessed from United States Geological Survey (USGS) website.

References

Aina, Y. A., Adam, E. M., & Ahmed, F. (2017). Spatiotemporal variations in the impacts of urban land use types on urban heat island effects : The case of Riyadh , Saudi Arabia. *Remote Sensing and Spatial Information Sciences*, *XLII*(May), 8–12.

Amiri, R., Alimohammadi, A., Kazem, S., & Panah, A. (2009). Spatial – temporal dynamics of land surface temperature in relation to fractional vegetation cover and land use / cover in the Tabriz urban area , Iran. *Remote Sensing of Environment*, *113*(February 2018), 2606–2617 Contents. https://doi.org/10.1016/j.rse.2009.07.021

Ayalew, D., Tesfaye, K., Mamo, G., Yitaferu, B., & Bayu, W. (2012). Variability of rainfall and its current trend in Amhara region , Ethiopia. *African Journal of Agricultural Research*, *7*(10), 1475–1486. https://doi.org/10.5897/AJAR11.698

Belay, A. S., Fenta, A. A., Yenehun, A., Nigate, F., Tilahun, S. A., Moges, M. M., Dessie, M., Adgo, E., Nyssen, J., Chen, M., Griensven, A. Van, & Walraevens, K. (2019). Evaluation and Application of Multi-Source Satellite Rainfall Product CHIRPS to Assess Spatio-Temporal Rainfall Variability on Data-Sparse Western Margins of Ethiopian Highlands. *Remote Sens*, *11*, 1–22.

Berger, C., Rosentreter, J., Voltersen, M., Baumgart, C., Schmullius, C., & Hese, S. (2017). Remote Sensing of Environment Spatio-temporal analysis of the relationship between 2D / 3D urban site characteristics and land surface temperature. *Remote Sensing of Environment*, *193*, 225–243. https://doi.org/10.1016/j.rse.2017.02.020

Bosilovich, M. G. (2006). A comparison of MODIS land surface temperature with in situ observations. *Geographical Research Letters*, *33*(July), 1–5. https://doi.org/10.1029/2006GL027519

Cai, Y., Zhang, H., Zheng, P., & Pan, W. (2016). Quantifying the Impact of Land use / Land Cover Changes on the Urban Heat Island : A Case Study of the Natural Wetlands Distribution Area of Fuzhou. *Wetlands*, *7*, 1–14. https://doi.org/10.1007/s13157-016-0738-7

Chen, X., Zhang, X., Church, J. A., Watson, C. S., King, M. A., Monselesan, D., Legresy, B., & Harig, C. (2017). The increasing rate of global mean sea-level rise during 1993 – 2014. *Nature and Climate Change*, *June*, 1–6. https://doi.org/10.1038/NCLIMATE3325

Fabeku, B. B., & Balogun, I. A. (2018). Spatio-Temporal Variability in Land Surface Temperature and Its Relationship with Vegetation Types over Ibadan , South-Western. *Atmospheric and Climate Sciences*, *8*, 318–336. https://doi.org/10.4236/acs.2018.83021

Farina, A. (2012). *Exploring the relationship between land surface temperature and vegetation abundance for urban heat island mitigation in Seville , Spain*.

Fernandes, R., & Leblanc, S. G. (2005). Parametric (modified least squares) and non-parametric (Theil-Sen) linear regressions for predicting biophysical parameters in the presence of measurement errors. *Remote Sensing of Environment*, *95*(3), 303–316. https://doi.org/10.1016/j.rse.2005.01.005

Gidey, E., Dikinya, O., Sebego, R., Segosebe, E., & Zenebe, A. (2018). Analysis of the long - term agricultural drought onset , cessation , duration , frequency , severity and spatial extent using Vegetation Health Index (VHI) in Raya and its environs , Northern Ethiopia. *Environmental Systems Research*, *7*, 1–18. https://doi.org/10.1186/s40068-018-0115-z

Güneralp, B., Zhou, Y., Ürge-Vorsatz, D., Gupta, M., Yu, S., Patel, P. L., Fragkias, M., Li, X., &

Seto, K. C. (2017). Global scenarios of urban density and its impacts on building energy use through 2050. *Proceedings of the National Academy of Sciences of the United States of America*, *114*(34), 8945–8950. https://doi.org/10.1073/pnas.1606035114

He, J., Zhao, W., Li, A., Wen, F., & Yu, D. (2018). The impact of the terrain effect on land surface temperature variation based on Landsat-8 observations in mountainous areas. *International Journal of Remote Sensing*, *40*(5–6), 1808–1827. https://doi.org/10.1080/01431161.2018.1466082

Ibitoye, M. ., Aderibigbe, O.G Adegoyega, S. ., & Adebola, A. . (2017). Spatio-Temporal Analysis of Land Surface Temperature variations in the rapidly developing Akure and its environs, Southwestern Nigeria using landsat data. *Ethiopian Journal of Environmental Studies & Management*, *10*(3), 389–403.

Jiang, Y., Fu, P., & Weng, Q. (2015). Assessing the Impacts of Urbanization-Associated Land Use/Cover Change on Land Surface Temperature and Surface Moisture: A Case Study in the Midwestern United States. *Remote Sens*, *7*, 4880–4898. https://doi.org/10.3390/rs70404880

Julien, Y., & Sobrino, J. A. (2009). Author ' s personal copy Comparison of cloud-reconstruction methods for time series of composite NDVI data. *Remote Sensing of Environment Journal*, *114*, 1–9. https://doi.org/10.1016/j.rse.2009.11.001

Julien, Y., Sobrino, J. A., & Verhoef, W. (2006). Changes in land surface temperatures and NDVI values over Europe between 1982 and 1999. *Remote Sensing of Environment*, *103*, 43–55. https://doi.org/10.1016/j.rse.2006.03.011

Justice, C. O., Vermote, E., Townshend, J. R. G., Defries, R., Roy, D. P., Hall, D. K., Salomonson, V. V., Privette, J. L., Riggs, G., Strahler, A., Lucht, W., Myneni, R. B., Knyazikhin, Y., Running, S. W., Nemani, R. R., Wan, Z., Huete, A. R., Van Leeuwen, W., Wolfe, R. E., … Barnsley, M. J. (1998). The moderate resolution imaging spectroradiometer (MODIS): Land remote sensing for global change research. *IEEE Transactions on Geoscience and Remote Sensing*, *36*(4), 1228–1249. https://doi.org/10.1109/36.701075

Khanal, S., Kc, K., Fulton, J. P., Shearer, S., & Ozkan, E. (2020). Remote Sensing in Agriculture Accomplishments , Limitations , and Opportunities. *Remote Sensing*, *12*, 1–29.

Khandelwal, S., Goyal, R., Kaul, N., & Mathew, A. (2017). Assessment of land surface temperature variation due to change in elevation of area surrounding Jaipur, India. *Egyptian Journal of Remote Sensing and Space Science*, *21*(1), 87–94. https://doi.org/10.1016/j.ejrs.2017.01.005

Khorchani, M., Vicente-serrano, S. M., Azorin-, C., Garcia, M., Martin-hernandez, N., Peña-, M., Kenawy, A. El, & Domínguez-castro, F. (2018). Trends in LST over the peninsular Spain as derived from the AVHRR imagery data Makki. *Global and Planetary Change*, 1–55. https://doi.org/10.1016/j.gloplacha.2018.04.006

Li, J., Pei, Y., Zhao, S., Xiao, R., Sang, X., & Zhang, C. (2020). A review of remote sensing for environmental monitoring in China. *Remote Sensing*, *12*(7), 1–25. https://doi.org/10.3390/rs12071130

Li, X., Zhou, Y., Asrar, G. R., & Zhu, Z. (2018). Creating a seamless 1 km resolution daily land surface temperature dataset for urban and surrounding areas in the conterminous United States. *Remote Sensing of Environment*, *206*(December 2017), 84–97. https://doi.org/10.1016/j.rse.2017.12.010

Li, Z., Tang, B., Wu, H., Ren, H., Yan, G., Wan, Z., Trigo, I. F., & Sobrino, J. A. (2013).

Remote Sensing of Environment Satellite-derived land surface temperature : Current status and perspectives. *Remote Sensing of Environment*, *131*, 14–37. https://doi.org/10.1016/j.rse.2012.12.008

Liang, L., Sun, Q., Luo, X., Wang, J., Zhang, L., Deng, M., Di, L., & Liu, Z. (2017). Long-term spatial and temporal variations of vegetative drought based on vegetation condition index in China. *Ecosphere*, *8*(8). https://doi.org/10.1002/ecs2.1919

Libiseller, C., & Grimvall, A. (2002). Performance of partial Mann-Kendall tests for trend detection in the presence of covariates. *Environmetrics*, *13*(1), 71–84. https://doi.org/10.1002/env.507

Luintel, N., Ma, W., Ma, Y., Wang, B., & Subba, S. (2019). Spatial and temporal variation of daytime and nighttime MODIS land surface temperature across Nepal Spatial and temporal variation of daytime and nighttime MODIS land surface. *Atmospheric and Oceanic Science Letters*, *12*(5), 305–312. https://doi.org/10.1080/16742834.2019.1625701

Maffei, C., Alfieri, S. M., & Menenti, M. (2018). Relating spatiotemporal patterns of forest fires burned area and duration to diurnal land surface temperature anomalies. *Remote Sens*, *10*(11), 1–20. https://doi.org/10.3390/rs10111777

Mann, H. B. (1945). Nonparametric tests against trend. *Econometrica*, *13*(3), 245–259.

Mesbah, L. H. M. (2013). Detecting hydro-climatic change using spatiotemporal analysis of rainfall time series in Western Algeria. *Nat Hazards*, *65*, 1293–1311. https://doi.org/10.1007/s11069-012-0411-2

Mildrexler, D. J., Cohen, W. B., & Running, S. W. (2018). ScholarWorks at University of Montana Thermal Anomalies Detect Critical Global Land Surface Changes Let us know how access to this document benefits you . *Journal of Applied Meteorology and Climatology*, *57*, 391–411.

Miles, V., & Esau, I. (2020). Urban Climate Surface urban heat islands in 57 cities across different climates in northern Fennoscandia. *Urban Climate*, *31*(August 2019), 100575. https://doi.org/10.1016/j.uclim.2019.100575

Mirzaei, M., Verrelst, J., Arbabi, M., & Shaklabadi, Z. (2020). Urban Heat Island Monitoring and Impacts on Citizen ' s General Health Status in Isfahan Metropolis : A Remote Sensing and Field Survey Approach. *Remote Sensing*, *12*(April), 1–17.

Muthoni, F. K., Odongo, V. O., Ochieng, J., Mugalavai, E. M., Mourice, S. K., Hoesche-zeledon, I., Mwila, M., & Bekunda, M. (2019). Long-term spatial-temporal trends and variability of rainfall over Eastern and Southern Africa. *Theoretical and Applied Climatology*, *137*, 1869–1882.

Ngie, A., Abutaleb, K., Ahmed, F., Darwish, A., & Ahmed, M. (2014). Assessment of urban heat island using satellite remotely sensed imagery : a review. *South African Geographical Journal*, *July*, 1–20. https://doi.org/10.1080/03736245.2014.924864

Noureldeen, N., Mao, K., Yuan, Z., Shen, X., Xu, T., & Qin, Z. (2017). Analysis of the Spatiotemporal Change in Land Surface Temperature for a Long-Term Sequence in. *Remote Sens*, *12*, 1–24.

NourEldeen, N., Mao, K., Yuan, Z., Shen, X., Xu, T., & Qin, Z. (2020). Analysis of the spatiotemporal change in land surface temperature for a long-term sequence in Africa (2003-2017). *Remote Sensing*, *12*(3), 1–25. https://doi.org/10.3390/rs12030488

Parvez, I. M., Aina, Y. A., & Balogun, A. (2019). The influence of urban form on the spatiotemporal variations in land surface temperature in an arid coastal city. *Geocarto International*, *0*(0), 1–21. https://doi.org/10.1080/10106049.2019.1622598

Peng, J., Ma, J., Liu, Q., Liu, Y., Hu, Y., Li, Y., & Yue, Y. (2018). Spatial-temporal change of land surface temperature across 285 cities in China: An urban-rural contrast perspective. *Science of the Total Environment*, *635*, 487–497. https://doi.org/10.1016/j.scitotenv.2018.04.105

Peng, X., Wu, W., Zheng, Y., Sun, J., Hu, T., & Wang, P. (2020). Correlation analysis of land surface temperature and topographic elements in Hangzhou , China. *Scientific Reports*, *10*, 1–16. https://doi.org/10.1038/s41598-020-67423-6

Phan, T. N., Kappas, M., & Tran, T. P. (2018). Land surface temperature variation due to changes in elevation in Northwest Vietnam. *Climate*, *6*(2), 1–19. https://doi.org/10.3390/cli6020028

Porter, P. S., Rao, S. T., & Hogrefe, C. (2002). Linear trend analysis: A comparison of methods. *Atmospheric Environment*, *36*(18), 3055–3056. https://doi.org/10.1016/S1352-2310(02)00189-9

Qian, X., Liang, L., Shen, Q., Sun, Q., Zhang, L., Liu, Z., Zhao, S., & Qin, Z. (2016). Drought trends based on the VCI and its correlation with climate factors in the agricultural areas of China from 1982 to 2010. *Environmental Monitoring and Assessment*, *188*(11). https://doi.org/10.1007/s10661-016-5657-9

Qiao, Z., Liu, L., Qin, Y., Xu, X., Wang, B., & Liu, Z. (2020). The Impact of Urban Renewal on Land Surface Temperature Changes : A Case Study in the Main City. *Remote Sens*, *12*, 1–15.

Qureshi, S., Alavipanah, S. K., Konyushkova, M., Mijani, N., Fathololomi, S., Firozjaei, M. K., Homaee, M., Hamzeh, S., & Kakroodi, A. A. (2020). A remotely sensed assessment of surface ecological change over the Gomishan Wetland, Iran. *Remote Sensing*, *12*(18), 1–24. https://doi.org/10.3390/RS12182989

Sen, P. K. (1968). Estimates of the Regression Coefficient Based on Kendall's Tau. *Journa lof the American Statistical Association.*, *63*(324), 1379–1389.

Shwetha, H. R., & Kumar, D. N. (2016). Prediction of high spatio-temporal resolution land surface temperature under cloudy conditions using microwave vegetation index and ANN. *ISPRS Journal of Photogrammetry and Remote Sensing*, *117*, 40–55. https://doi.org/10.1016/j.isprsjprs.2016.03.011

Singh, R. B., Grover, A., & Zhan, J. (2014). Inter-Seasonal Variations of Surface Temperature in the Urbanized Environment of Delhi Using Landsat Thermal Data. *Energies*, *7*, 1811–1828. https://doi.org/10.3390/en7031811

Thorne, P. W., Donat, M. G., Dunn, R. J. H., Williams, C. N., Alexander, L. V, Caesar, J., Durre, I., Harris, I., Hausfather, Z., Jones, P. D., Menne, M. J., Rohde, R., Vose, R. S., Davy, R., Lawrimore, J. H., Peterson, T. C., & Rennie, J. J. (2016). Journal of Geophysical Research : Atmospheres. *Journal of Geophysical Research: Atmospheres RESEARCH*, *121*, 5138–5158. https://doi.org/10.1002/2015JD024584.Received

Tomlinson, C. J., Chapman, L., Thornes, E., & Baker, C. (2011). Remote sensing land surface temperature for meteorology and climatology : a review. *Remote Sensing Land Surface Temperature*, *306*, 296–306. https://doi.org/10.1002/met.287

Xiao, H., Kopeck, M., Guo, S., Guan, Y., Cai, D., & Zhang, C. (2018). Responses of Urban Land Surface Temperature on Land Cover : A Comparative Study of Vienna and Madrid. *Sustainability Article*, *10*, 260. https://doi.org/10.3390/su10020260

Yang, C., Zhan, Q., Gao, S., & Liu, H. (2020). Geo-spatial Information Science Characterizing the spatial and temporal variation of the land surface temperature hotspots in Wuhan from a

local scale. *Geo-Spatial Information Science*, *23*(4), 327–340. https://doi.org/10.1080/10095020.2020.1834882

Yang, H., Xi, C., Zhao, X., Mao, P., & Wang, Z. (2020). Measuring the Urban Land Surface Temperature Variations Under Zhengzhou City Expansion Using Landsat-Like Data. *Remote Sens*, *12*, 1–21.

Ye, C., Wang, M., & Li, J. (2017). Derivation of the characteristics of the Surface Urban Heat Island in the Greater Toronto area using thermal infrared remote sensing Derivation of the characteristics of the Surface Urban Heat. *Remote Sensing Letters*, *8*(7), 637–646. https://doi.org/10.1080/2150704X.2017.1312025

Yue, S., Pilon, P., & Cavadias, G. (2002). Power of the Mann ± Kendall and Spearman ' s rho tests for detecting monotonic trends in hydrological series. *Journal of Hydrology*, *259*, 254–271.

Zhou, D., Li, D., Sun, G., Zhang, L., Liu, Y., & Hao, L. (2016). Journal of geophysical research. *Nature*, *175*(4449), 238. https://doi.org/10.1038/175238c0

Zhu, X., Wang, X., Yan, D., Liu, Z., & Zhou, Y. (2018). Analysis of remotely-sensed ecological indexes' influence on urban thermal environment dynamic using an integrated ecological index: a case study of Xi'an, China. *International Journal of Remote Sensing*, *40*(9), 3421–3447. https://doi.org/10.1080/01431161.2018.1547448

Figures

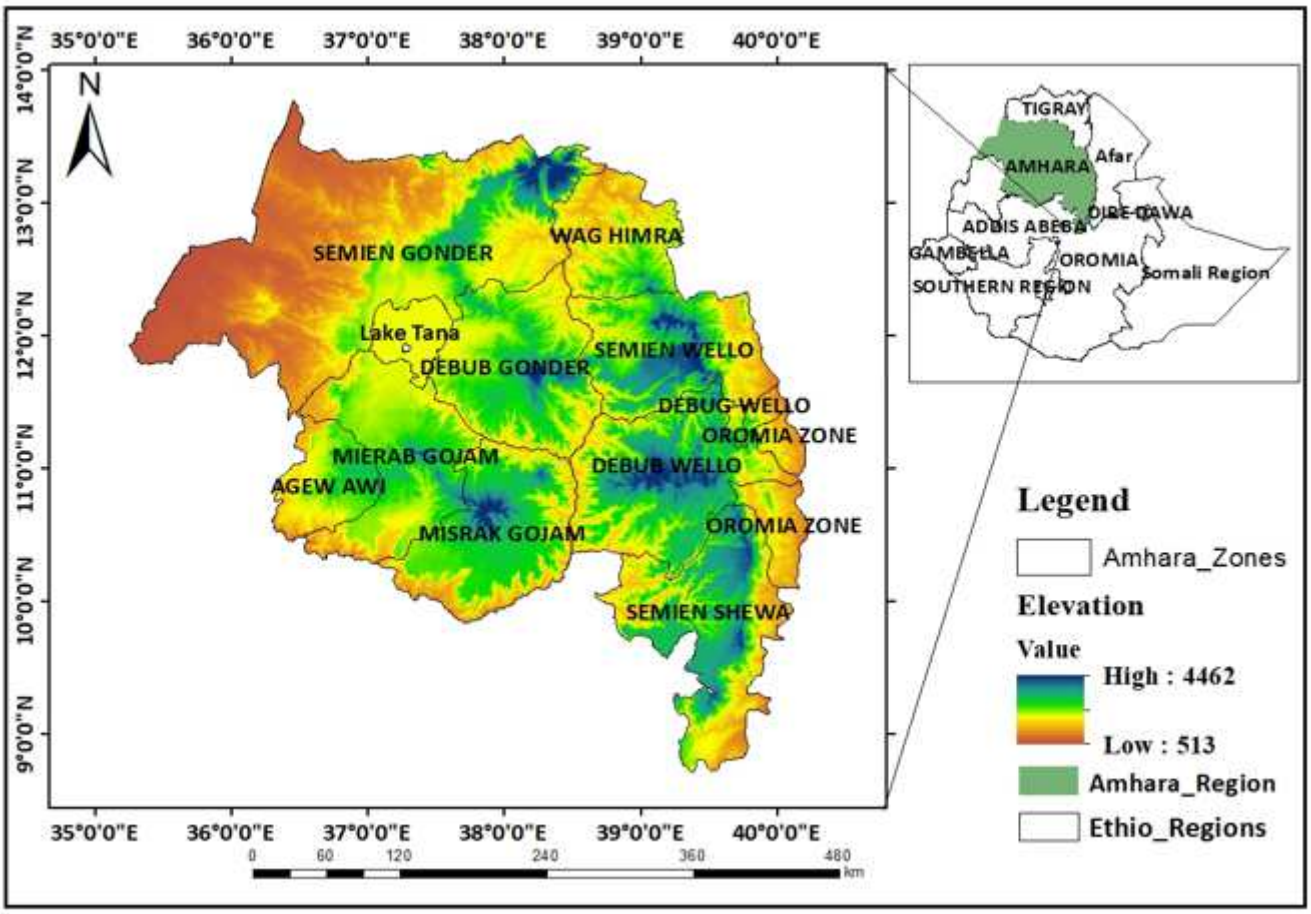

Figure 1

Location map of the study area

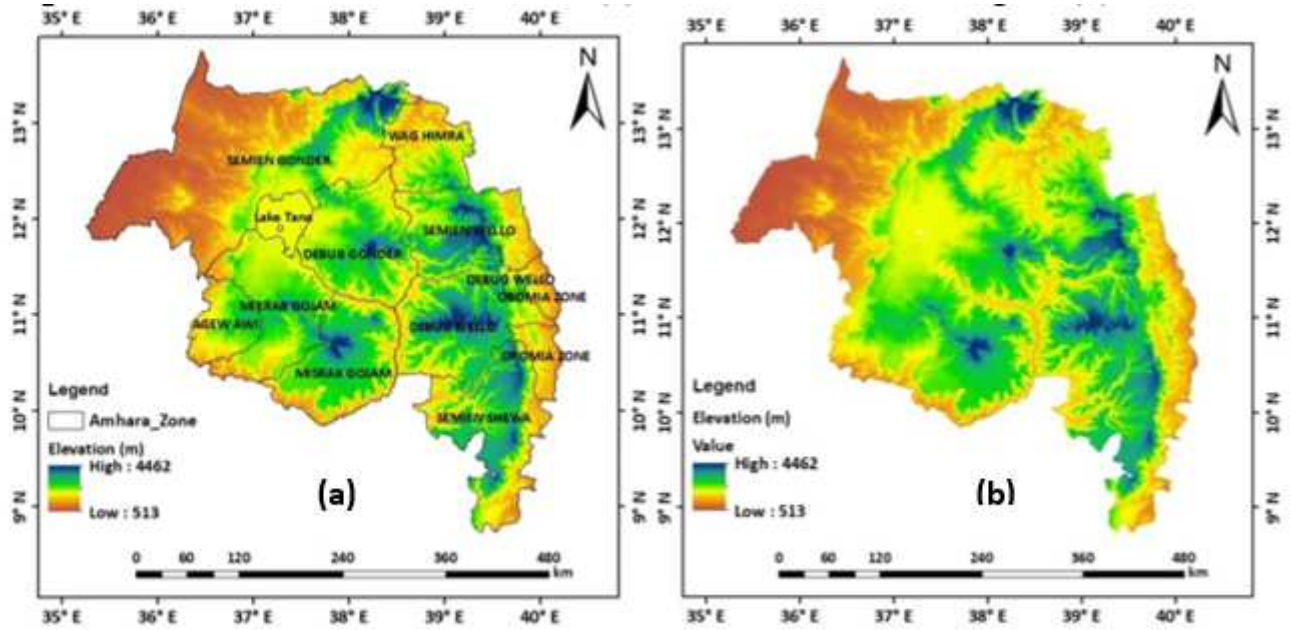

Figure 2

Elevation across different zone (a) and elevation of the region (b)

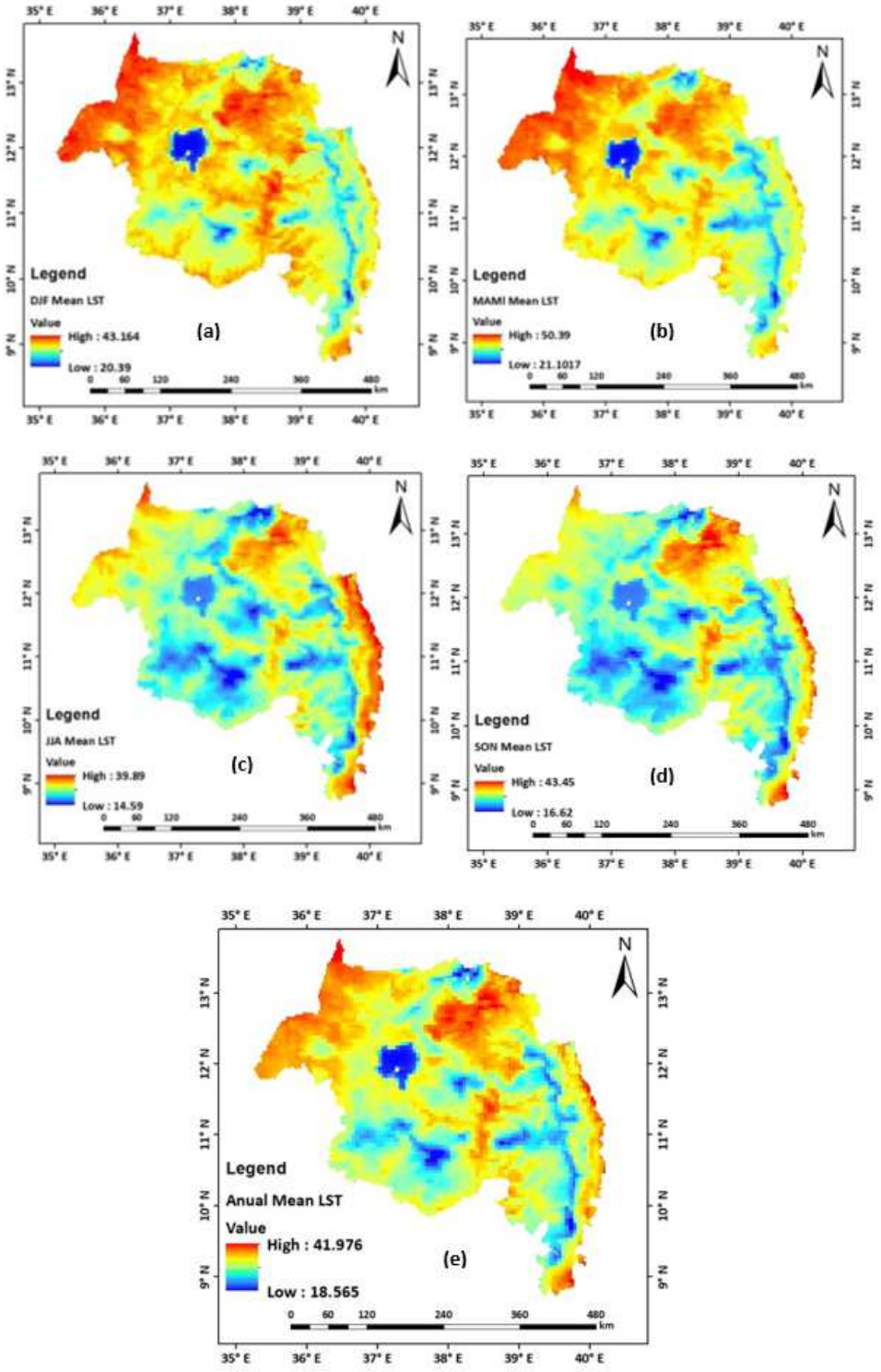

Figure 3

Spatial distribution of mean winter (DJF) LST (a) mean spring (MAM) LST (b) mean summer (JJA) LST (c) mean autumn (SON) LST (d) and mean annual LST (e) of Amhara Region (2001-2020)

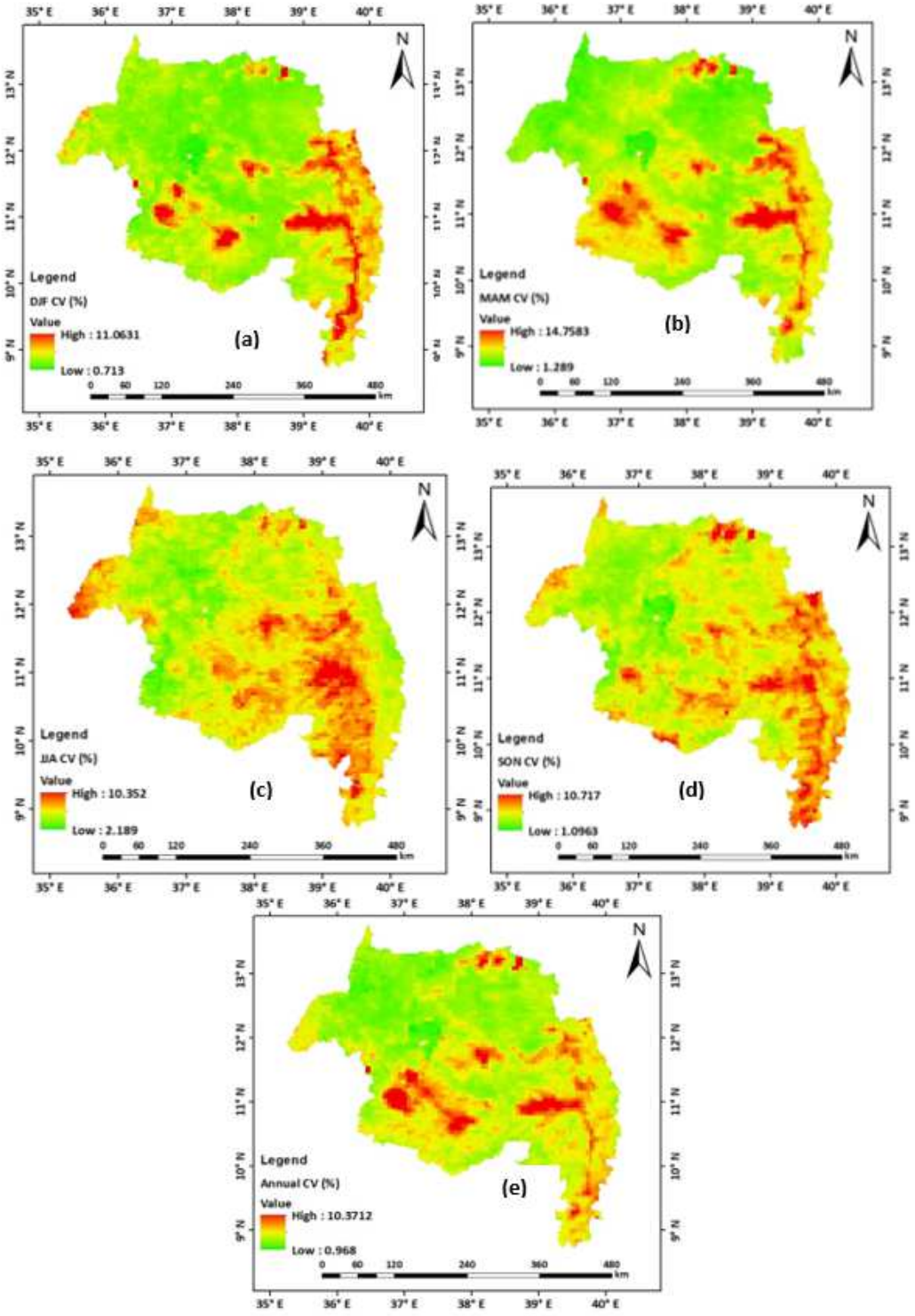

Figure 4

The spatial distribution of LST CV of the winter season (a) spring season (b) summer season (c) autumn season (d) and annual LST (e) of Amhara Region (2001-2020)

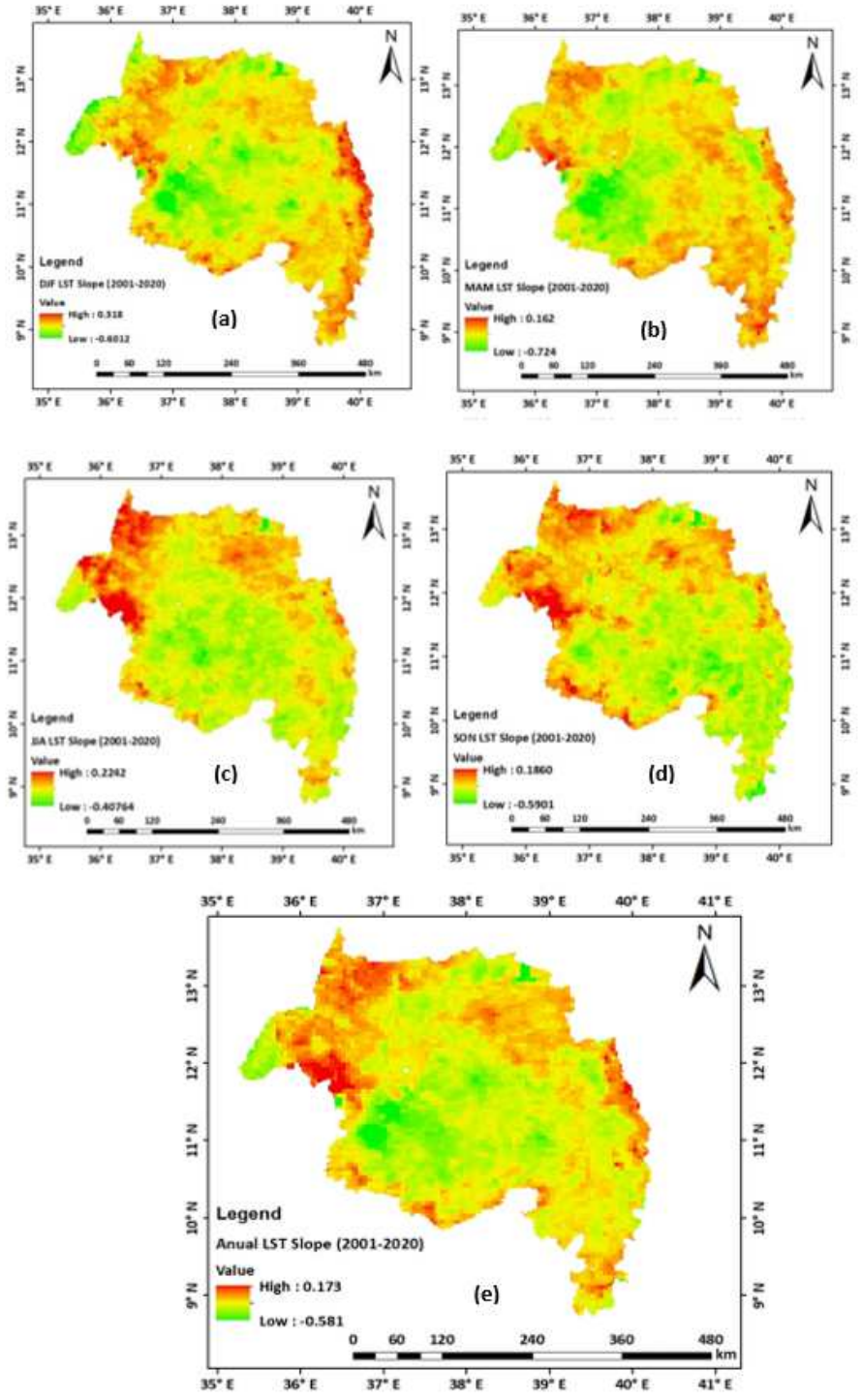

Figure 5

The spatial LST trend of winter season (a) spring season (b) summer season (c) autumn season (d) and annual LST (e) of Amhara Region (2001-2020)

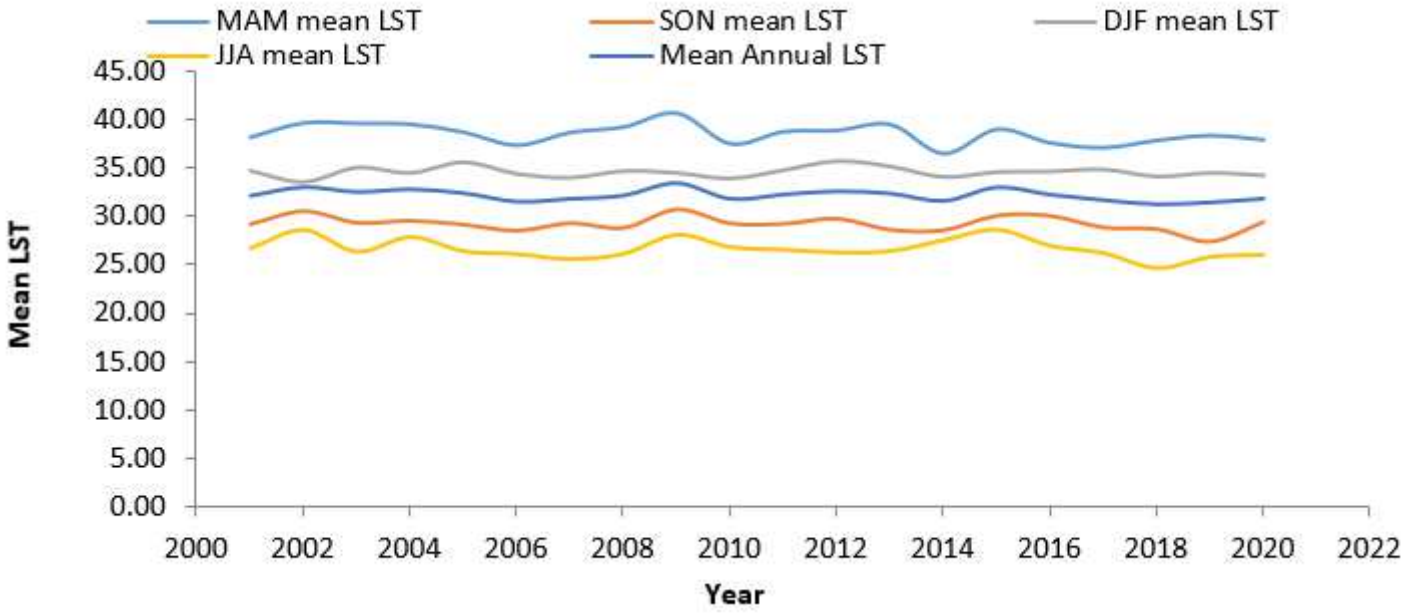

Figure 6

Yearly variation of mean seasonal and annual LST (2001-2020)

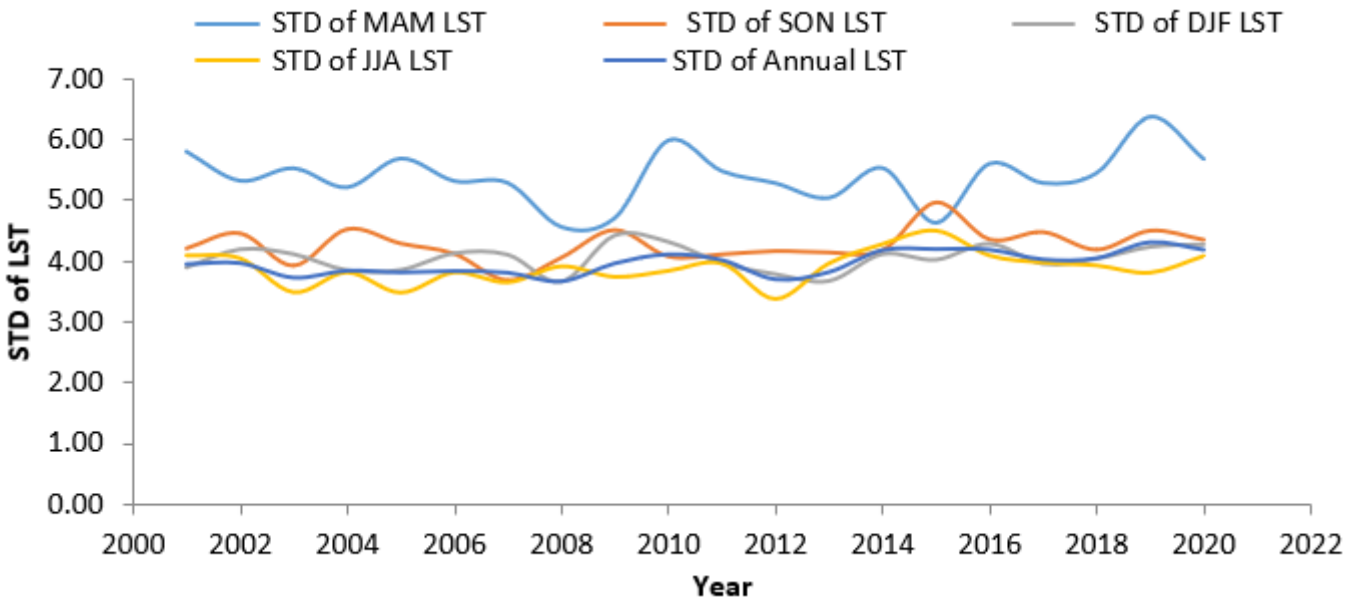

Figure 7

Inter-annual variability of seasonal and annual LST (2001-2020)